Predictions for p+Pb Collisions at $\sqrt{s_{NN}} = 5$ TeV: Expectations vs. Data

R. Vogt (with members and friends of the JET Collaboration)

Lawrence Livermore National Laboratory, Livermore, CA 94551, USA
Physics Department, University of California, Davis, CA 95616, USA

Int. J. Mod. Phys. E 22 (2013) 1330007 [arXiv:1301.3395 [hep-ph]],
update in progress

Contributions to calculations in this talk from: J. Albacete *et al.* (rcBK, charged hadrons), F. Arleo *et al.* (J/ψ, Υ), G. Barnafoldi *et al.* (charged hadrons, forward/backward asymmetry), K. J. Eskola ($R_{p\mathrm{Pb}}$, dijets), E. G. Ferreiro (J/ψ, ψ') H. Fujii *et al.* (J/ψ, Υ) B. Kopeliovich ($R_{p\mathrm{Pb}}$), J.-P. Lansberg *et al.* (J/ψ, Υ), Z. Lin (AMPT), A. Rezaeian (b-CGC charged hadrons), V. Topor Pop *et al.* (HIJINGB$\overline{\mathrm{B}}$), R. Venugopalan *et al.* (IP-Sat), I. Vitev *et al.* (jets), RV (J/ψ, Υ), X.-N. Wang *et al* (charged hadrons), B.-W. Zhang *et al* (gauge bosons),

U.S. DEPARTMENT OF ENERGY | Office of Science

Outline

We stick to results where data are already available

Model descriptions are combined with available data

- **Charged particles**
  - $dN_{\mathrm{ch}}/d\eta$
  - dN_{ch}/dp_T
  - $R_{p\mathrm{Pb}}(p_T)$
  - **Flow**
- **Jets**
  - **Dijets**
  - **Single inclusive jets**
- J/ψ **and** Υ
  - $R_{p\mathrm{Pb}}(y)$
  - $R_{F/B}(y)$, $R_{F/B}(p_T)$
- Z **bosons**

Model Descriptions

Saturation

Saturation: rcBK (A. Rezaeian, J. Albacete *et al*)

Gluon jet production in pA described by k_T-factorization

$$\frac{d\sigma}{dy\, d^2p_T} = \frac{2\alpha_s}{C_F}\frac{1}{p_T^2}\int d^2\vec{k}_T \phi_p^G\left(x_1;\vec{k}_T\right)\phi_A^G\left(x_2;\vec{p}_T-\vec{k}_T\right)$$

Here $x_{1,2} = (p_T/\sqrt{s})e^{\pm y}$ and unintegrated gluon density, $\phi_A^G(x_i;\vec{k}_T)$, is related to color dipole forward scattering amplitude

$$\begin{aligned}\phi_A^G\left(x_i;\vec{k}_T\right) &= \frac{1}{\alpha_s}\frac{C_F}{(2\pi)^3}\int d^2\vec{b}_T\, d^2\vec{r}_T\, e^{i\vec{k}_T\cdot\vec{r}_T}\,\nabla_T^2\mathcal{N}_A\left(x_i;r_T;b_T\right)\\ \mathcal{N}_A\left(x_i;r_T;b_T\right) &= 2\mathcal{N}_F\left(x_i;r_T;b_T\right)-\mathcal{N}_F^2\left(x_i;r_T;b_T\right)\end{aligned}$$

In k_T-factorized approach, both projectile and target have to be at small x so that CGC formalism is applicable to both

rcBK Hybrid Approach

Hybrid models that treat the projectile (forward) with DGLAP collinear factorization and target with CGC methods

Hadron cross section is proportional to $f_g(x_1,\mu_F^2)N_A(x_2,p_T/z)+f_q(x_1,\mu_F^2)N_F(x_2,p_T/z)$ **modulo fragmentation functions**

$$\begin{aligned}\frac{dN^{pA\to hX}}{d\eta d^2p_T} &= \frac{K}{(2\pi)^2}\Bigg[\int_{x_F}^1\frac{dz}{z^2}\Big[x_1f_g(x_1,\mu_F^2)N_A(x_2,\frac{p_T}{z})D_{h/g}(z,\mu_{\rm Fr})\\ &+ \Sigma_q x_1 f_q(x_1,\mu_F^2)N_F(x_2,\frac{p_T}{z})D_{h/q}(z,\mu_{\rm Fr})\Big]\\ &+ \frac{\alpha_s^{\rm in}}{2\pi^2}\int_{x_F}^1\frac{dz}{z^2}\frac{z^4}{p_T^4}\int_{k_T^2<\mu_F^2}d^2k_Tk_T^2N_F(k_T,x_2)\int_{x_1}^1\frac{d\xi}{\xi}\\ &\times \Sigma_{i,j=q,\bar q,g}w_{i/j}(\xi)P_{i/j}(\xi)x_1f_j(\frac{x_1}{\xi},\mu_F)D_{h/i}(z,\mu_{\rm Fr})\Bigg]\,.\end{aligned}$$

K **factor introduced to incorporate higher order corrections**

Inelastic term is multiplied by $\alpha_s^{\rm in}$**, different from running** α_s **in rcBK equation – in hybrid formulation, strong coupling in dilute regime (proton) can differ from that in the dense system (nucleus) but appropriate scale of** $\alpha_s^{\rm in}$ **cannot be determined without a NNLO calculation**

Factorization, renormalization and fragmentation scales assumed to be equal, $\mu_F=\mu_R=\mu_{\rm Fr}$ **with** $\mu_F=2p_T$**,** p_T **and** $p_T/2$ **to form uncertainty range for given** N **and** $\alpha_s^{\rm in}$

rcBK Equation

$N_{A(F)}$ is 2-D Fourier transform of imaginary part of dipole scattering amplitude in the fundamental (F) or adjoint (A) representation $\mathcal{N}_{A(F)}$

$\mathcal{N}_{A(F)}$ calculated using JIMWLK which simplifies to BK in the large N_c limit

Running coupling corrections to LL kernel result in rcBK equation

$$\begin{aligned}\frac{\partial \mathcal{N}_{A(F)}(r,x)}{\partial \ln(x_0/x)} &= \int d^2\vec{r}_1 \; K^{\rm run}(\vec{r},\vec{r}_1,\vec{r}_2)\left[\mathcal{N}_{A(F)}(r_1,x)+\mathcal{N}_{A(F)}(r_2,x)\right.\\ &- \left.\mathcal{N}_{A(F)}(r,x)-\mathcal{N}_{A(F)}(r_1,x)\,\mathcal{N}_{A(F)}(r_2,x)\right]\end{aligned}$$

$$\mathcal{N}(r,Y=0) = 1-\exp\left[-\frac{\left(r^2\,Q_{0s}^2\right)^\gamma}{4}\,\ln\left(\frac{1}{\Lambda\,r}+e\right)\right]$$

Last equation is initial condition with γ fixed from DIS data, $\gamma=1$ is MV initial condition, $\gamma\sim 1.1$ in fits

$Q_{0p}^2\sim 0.2$ GeV^2 in MV initial condition, smaller for other values of γ

$Q_{0A}^2\sim NQ_{0p}^2$ with $3<N<7$ in Rezaeian's calculations, Albacete *et al* let nuclear scale be proportional to the number of participants at a given b to account for geometrical fluctuations in Monte Carlo simulations

Saturation: IP-Sat (Tribedy and Venugopalan)

Here one starts as before with k_T-factorization

$$\frac{dN_g^{pA}(b_T)}{dy\ d^2p_T} = \frac{4\alpha_s}{\pi C_F}\frac{1}{p_T^2}\int\frac{d^2k_T}{(2\pi)^5}\int d^2s_T \frac{d\phi_p(x_1,k_T|s_T)}{d^2s_T}\frac{d\phi_A(x_2,p_T-k_T|s_T-b_T)}{d^2s_T}$$

Unintegrated gluon density is expressed in terms of the dipole cross section as

$$\frac{d\phi^{p,A}(x,k_T|s_T)}{d^2s_T} = \frac{k_T^2N_c}{4\alpha_s}\int_0^\infty d^2r_T e^{i\vec{k_T}.\vec{r_T}}\left[1-\frac{1}{2}\frac{d\sigma_{\rm dip}^{p,A}}{d^2s_T}(r_T,x,s_T)\right]^2$$

Dipole cross section is a refinement of Golec-Biernat–Wusthoff that gives the right perturbative limit for $r_T \to 0$, equivalent to effective theory of CGC to LL

$$\frac{d\sigma_{\rm dip}^{p}}{d^2b_T}(r_T,x,b_T) = 2\left[1-\exp\left(-\frac{\pi^2}{2N_c}r_T^2\alpha_s(\mu^2)xg(x,\mu^2)T_p(b_T)\right)\right]$$

μ^2 is related to dipole radius, r_T, by $\mu^2 = \frac{4}{r_T^2}+\mu_0^2$

The gluon density $g(x,\mu^2)$ is LO DGLAP result without quarks

$T_p(b_T)$ is the gluon density profile function, $T_p(b_T) = (2\pi B_G)^{-1}\exp\left[-(b_T^2/2B_G)\right]$ where $\langle b^2\rangle = 2B_G$, the average squared gluonic radius of the proton, obtained from HERA data

Event-by-Event Calculations

HIJING2.0 (X.-N. Wang *et al*)

Based on two-component model of hadron production, soft (string excitations with effective cross section $\sigma_{\rm soft}$) and hard (perturbative QCD) components separated by cutoff momentum p_0
LO pQCD calculation with K factor to absorb higher-order corrections

$$\frac{d\sigma_{pA}^{\rm jet}}{dy_1 d^2p_T} = K \int dy_2\, d^2b\, T_A(b) \sum_{a,b,c} x_1 f_{a/p}(x_1, p_T^2) x_2 f_{a/A}(x_2, p_T^2, b) \frac{d\sigma_{ab\to cd}}{dt}$$

Effective $2 \to 2$ scattering, $x_{1,2} = p_T(e^{\pm y_1} + e^{\pm y_2})/\sqrt{s}$

Default HIJING collisions decomposed into independent and sequential NN collisions – in each NN interaction, hard collisions simulated first, followed by soft

Since hard interactions occur over shorter time scale, HIJING2.0 also uses decoherent hard scattering (DHC) where all hard collisions are simulated first, then soft, so available energy unrestricted by soft interactions
Energy-dependent k_T broadening in HIJING

$$\langle k_T^2 \rangle = [0.14 \log(\sqrt{s}/\text{GeV}) - 0.43]\,\text{GeV}^2/c^2$$

Shadowing in HIJING

Shadowing treated as scale independent
Versions before HIJING2.0 did not differentiate between quark and gluon shadowing

$$
\begin{aligned}
f_{a/A}(x,\mu_F^2,b) &= S_{a/A}(x,\mu_F^2,b) f_{a/A}(x,\mu_F^2) \\
S_{a/A}(x) &\equiv \frac{f_{a/A}(x)}{A f_{a/N}(x)} \\
&= 1 + 1.19 \log^{1/6} A \left[x^3 - 1.2x^2 + 0.21x\right] \\
&\quad - s_a (A^{1/3}-1)^n \left[1 - \frac{10.8}{\log(A+1)}\sqrt{x}\right] e^{-x^2/0.01} \\
s_a(b) &= s_a \frac{5}{3}\left(1 - \frac{b^2}{R_A^2}\right)
\end{aligned}
$$

In HIJING2.0 the $(A^{1/3}-1)$ factor is nonlinear ($n = 0.6$) but $n = 1$ in earlier versions

Previously $s_a = s_g = s_q = 0.1$

In HIJING2.0 $s_g \neq s_q$: $s_q = 0.1$ and $s_g \sim 0.22 - 0.23$ to match LHC data

The b dependence of s_a gives some impact parameter dependence to $S_{a/A}$

HIJINGB$\overline{\text{B}}$ (V. Topor Pop *et al*)

Differs from standard HIJING in treatment of fragmentation

HIJING uses string fragmentation with constant vacuum value of $\kappa_0 = 1.0$ GeV/fm for string tension

HIJINGB$\overline{\text{B}}$ allows for multiple overlapping flux tubes leading to strong longitudinal color field (SCF) effects

SCF effects modeled by varying κ and momentum cutoff with $\sqrt{s}$ and A

Fragmentation also modified, including baryon loops to explain baryon to meson anomaly and increase strange baryon production

AMPT: A Multi-Phase Transport (Z. Lin)

AMPT is a Monte Carlo transport model for heavy ion collisions, montage of other codes

- Heavy Ion Jet Interaction Generator (HIJING) for generating the initial conditions
- Zhang's Parton Cascade (ZPC) for modeling partonic scatterings
- A Relativistic Transport (ART) model for treating hadronic scatterings

AMPT – def treats the initial condition as strings and minijets and using Lund string fragmentation

AMPT – SM treats the initial condition as partons and uses a simple coalescence model to describe hadronization

Perturbative QCD Calculations

Leading Order Calculations (I. Vitev *et al*)

LO single inclusive hadron production cross section

$$\frac{d\sigma}{dyd^2p_T} = K\frac{\alpha_s^2}{s}\sum_{a,b,c}\int\frac{dx_1}{x_1}d^2k_{T_1}\,f_{a/N}(x_1,k_{T_1}^2)\int\frac{dx_2}{x_2}d^2k_{T_2}\,f_{b/N}(x_2,k_{T_2}^2)$$
$$\times\int\frac{dz_c}{z_c^2}\,D_{h/c}(z_c)H_{ab\to c}(\hat{s},\hat{t},\hat{u})\delta(\hat{s}+\hat{t}+\hat{u})$$

Gaussian form of k_T dependence in parton densities assumed

$$f_{a/N}(x_1,k_{T_1}^2) = f_{a/N}(x_1)\frac{1}{\pi\langle k_T^2\rangle}e^{-k_{T_1}^2/\langle k_T^2\rangle}$$

In pp collisions, $\langle k_T^2\rangle_{pp} = 1.8$ GeV$^2/c^2$

Broadening increased in cold matter, $\langle k_T^2\rangle_{pA} = \langle k_T^2\rangle_{pp} + \langle 2\mu^2 L/\lambda_{q,g}\rangle\zeta$

Cold matter energy loss due to medium-induced gluon Bremsstrahlung, implemented as a shift in momentum fraction, $f_{i/p}(x) \longrightarrow f_{i/p}(x/(1-\epsilon_{i,\mathrm{eff}}))$ where $\epsilon \propto \Sigma_i\Delta E_i/E$ with the sum over all medium-induced gluons

Dynamical shadowing shifts nuclear parton momentum fraction so that $f_{i/p}(x) \longrightarrow f_{i/p}((x/-\hat{t})(1+C_i\zeta_i^2(A^{1/3}-1))$

Proton and neutron number (isospin) accounted for

LO/NLO pQCD, w/out Energy Loss (G. Barnafoldi *et al*)

`kTpQCD_v2.0` assumes collinear factorization up to NLO

$$
\begin{aligned}
E_h \frac{d\sigma_h^{pp}}{d^3 p_T} &= \frac{1}{s} \sum_{abc} \int_{VW/z_c}^{1-(1-V)/z_c} \frac{dv}{v(1-v)} \int_{VW/vz_c}^{1} \frac{dw}{w} \int^{1} dz_c \\
&\times \int d^2\vec{k}_{T_1} \int d^2\vec{k}_{T_2}\; f_{a/p}(x_1, \vec{k}_{T_1}, \mu_F^2)\, f_{b/p}(x_2, \vec{k}_{T_2}, \mu_F^2) \\
&\times \left[\frac{d\widetilde{\sigma}}{dv} \delta(1-w) + \frac{\alpha_s(\mu_R)}{\pi} K_{ab,c}(\hat{s}, v, w, \mu_F, \mu_R, \mu_{\rm Fr}) \right] \frac{D_c^h(z_c, \mu_{\rm Fr}^2)}{\pi z_c^2} \; .
\end{aligned}
$$

$d\widetilde{\sigma}/dv$ is LO cross section with next-order correction term $K_{ab,c}(\hat{s}, v, w, \mu_F, \mu_R, \mu_{\rm Fr})$

Proton and parton level NLO kinematic variables are (s, V, W) and ($\hat{s}$, v, w)

k_T broadening implemented similar to previous LO calculation with

$$
\langle k_T^2 \rangle_{pA} = \langle k_T^2 \rangle_{pp} + C h_{pA}(b)
$$

$$
h_{pA}(b) = \begin{cases} \nu_A(b) - 1 & \nu_A(b) < \nu_m \\ \nu_m - 1 & \text{otherwise} \end{cases}
$$

Shadowing implemented through available parameterizations: EKS98, EPS08, HKN, and `HIJING2.0` – scale dependence included

$$
f_{a/A}(x, \mu_F^2) = S_{a/A}(x, \mu_F^2) \left[\frac{Z}{A} f_{a/p}(x, \mu_F^2) + \left(1 - \frac{Z}{A} \right) f_{a/n}(x, \mu_F^2) \right]
$$

NLO Shadowing Calculation (K. J. Eskola *et al*)

Calculate π^0 production at NLO, compared to charged particle R_{AA}

Only modifications of the parton PDFs in nuclei included

Improved spatial dependence of nPDFs on both EKS98 and EPS09 using power series expansion in the nuclear thickness function

$$r_i^A(x, Q^2, \mathbf{s}) = 1 + \sum_{j=1}^{n} c_j^i(x, Q^2) \left[T_A(\mathbf{s})\right]^j$$

They use the A dependence of the global (min bias) nPDFs to fix coefficients c_j^i

Found $n = 4$ sufficient for reproducing the A systematics

Used INCNLO package with CTEQ6M and KKP, AKK and fDSS fragmentation functions, uncertainties calculated with EPS09(s) error sets and fDSS

The modification factor $R_{p\mathrm{Pb}}$ is calculated as

$$R_{p\mathrm{Pb}}^{\pi^0}(p_T, y; b_1, b_2) \equiv \frac{\left\langle \dfrac{d^2N_{p\mathrm{Pb}}^{\pi^0}}{dp_T dy} \right\rangle_{b_1,b_2}}{\dfrac{\langle N_{\mathrm{coll}}^{p\mathrm{Pb}} \rangle_{b_1,b_2}}{\sigma_{\mathrm{in}}^{NN}} \dfrac{d^2\sigma_{\mathrm{pp}}^{\pi^0}}{dp_T dy}} = \frac{\int_{b_1}^{b_2} d^2\mathbf{b} \dfrac{d^2N_{p\mathrm{Pb}}^{\pi^0}(\mathbf{b})}{dp_T dy}}{\int_{b_1}^{b_2} d^2\mathbf{b}\, T_{p\mathrm{Pb}}(\mathbf{b}) \dfrac{d^2\sigma_{\mathrm{pp}}^{\pi^0}}{dp_T dy}}$$

b_1 and b_2 are centrality-based limits with $b_1 = 0$ and $b_2 \to \infty$ in min bias collisions

Charged particle and π^0 $R_{p\mathrm{Pb}}$ may be different because of greater baryon contribution in pA collisions, at least in some parts of phase space

Charged Particle Multiplicity and p_T Distributions: Midrapidity

$dN_{\rm ch}/d\eta$ in Lab Frame

Most calculations done in CM Frame, shift to lab frame involves a shift of $\Delta y_{NN} = 0.465$ in the direction of the proton beam

Test beam data taken with Pb beam moving toward forward rapidity (to the right)

Data do not favor saturation, slope from p side to Pb side is too steep (see next slide)

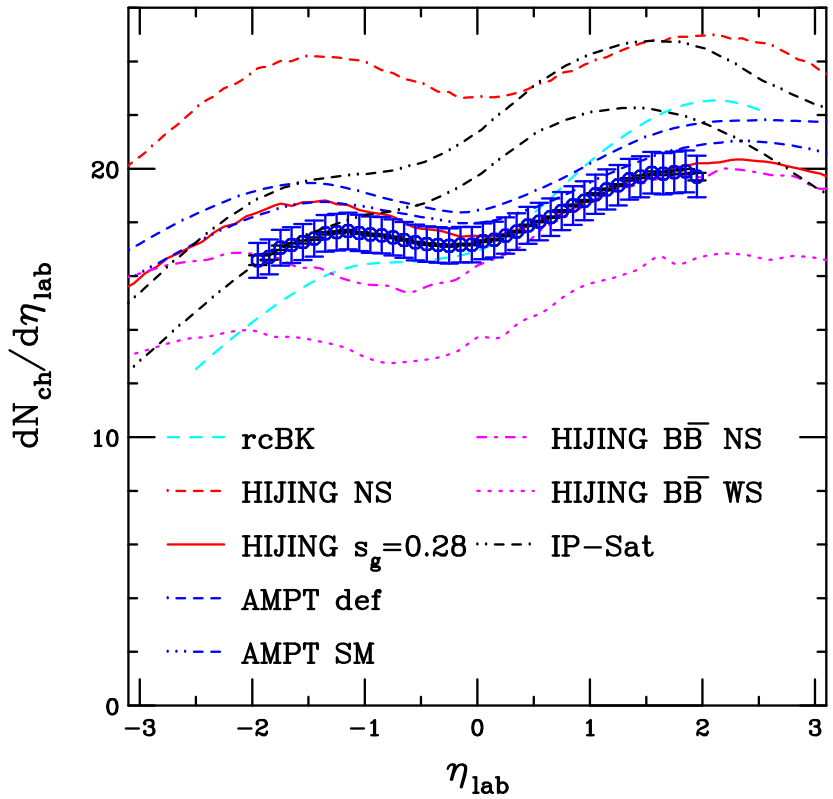

Figure 1: **Charged particle pseudorapidity distributions at $\sqrt{s_{NN}} = 5.02$ TeV in the lab frame. Calculations by Albacete *et al.*, XN Wang *et al.*, Z Lin, Rezaeian, and Topor Pop *et al.* The ALICE data (Phys. Rev. Lett. 110 (2013) 082302) are shown.**

CGC Results Depend on Jacobian

The slope of $dN_{\rm ch}/d\eta$ depends on the Jacobian $y \to \eta$ transformation

Previous calculations assumed the same Jacobian in pp and p+Pb collisions

New results based on 'tuned' Jacobian shows the sensitivity of $dN_{\rm ch}/d\eta$ to mass and p_T of final-state hadrons (note also that the convention is changed, proton beam has positive y)

Fixed minijet mass (related to pre-handronization/fragmentation stage) is assumed – can't be extracted in CGC, problem largest on the nuclear side

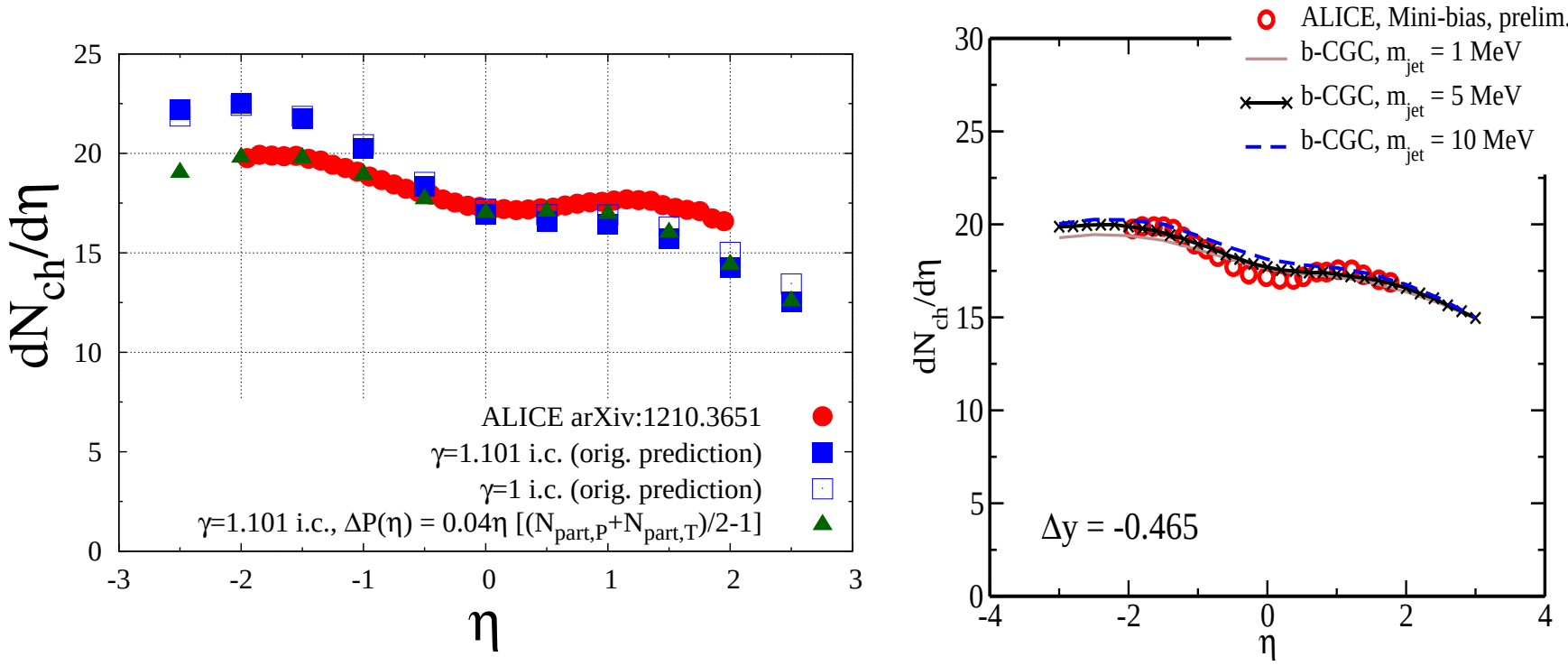

Figure 2: **Charged particle pseudorapidity distributions at $\sqrt{s_{NN}} = 5.02$ TeV with and without tuned Jacobian compared to the ALICE data (Phys. Rev. Lett. 110 (2013) 082302). Calculations by Albacete *et al.* with $\Delta P(\eta)$ are shown on the left-hand side, results changing the minijet mass in b-CGC by Rezaeian are shown on the right-hand side. Note that here the proton moves to the right (positive y).**

Centrality Dependence of $dN_{\rm ch}/d\eta$

Left-hand side compares `AMPT – def` (Z. Lin) to ATLAS data

Right-hand side shows the comparison with b-CGC: saturation scale modified to depend on impact parameter (A. Rezaeian)

Results are qualitatively similar but b-CGC more linear than data in more central collisions

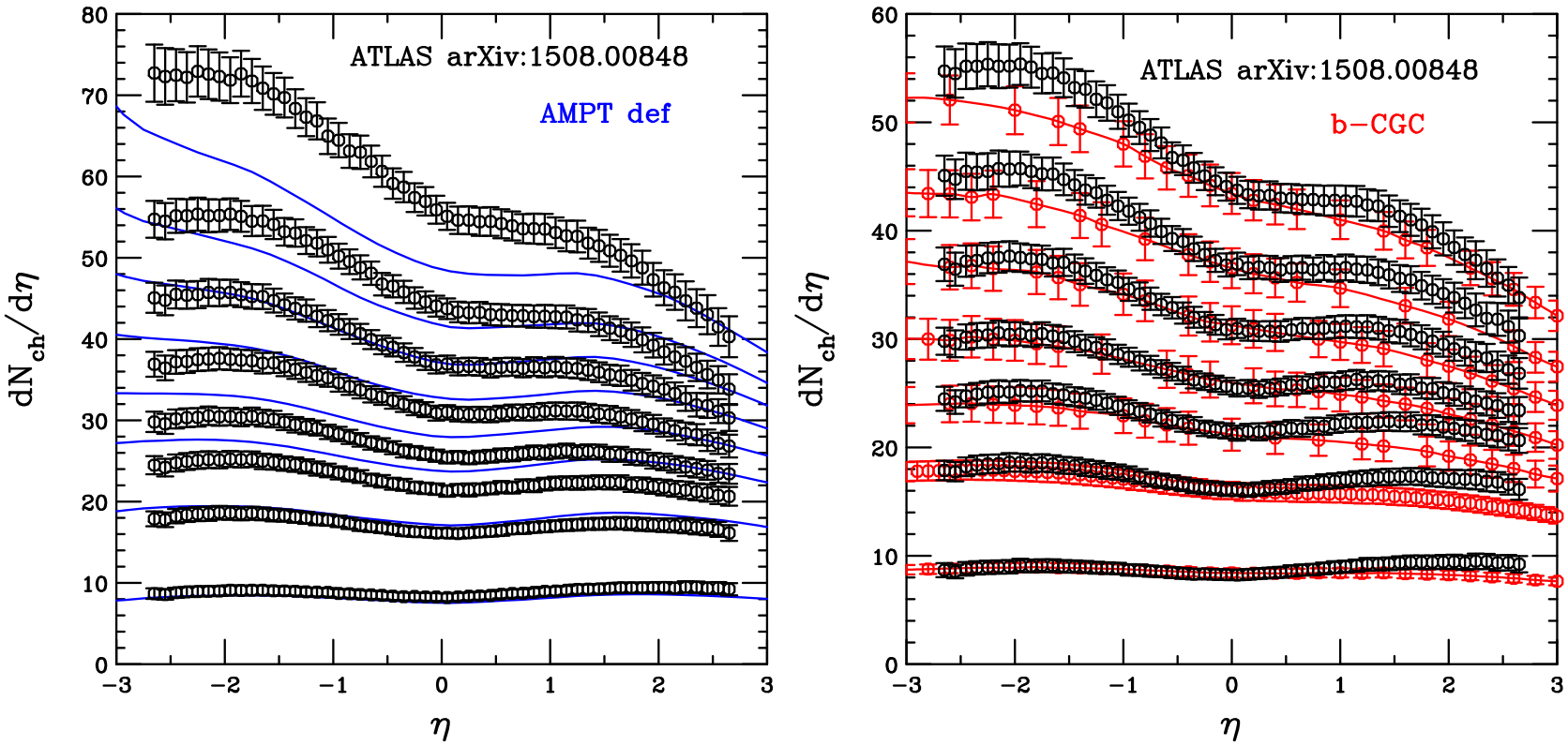

Figure 3: **The ATLAS multiplicity distributions (arXiv:1508.00848), binned in centrality, are compared to calculations with `AMPT – def` by Lin (left) and b-CGC by Rezaeian (right). There is no 0-1% b-CGC centrality calculation.**

$R_{p\mathrm{Pb}}$ at Midrapidity

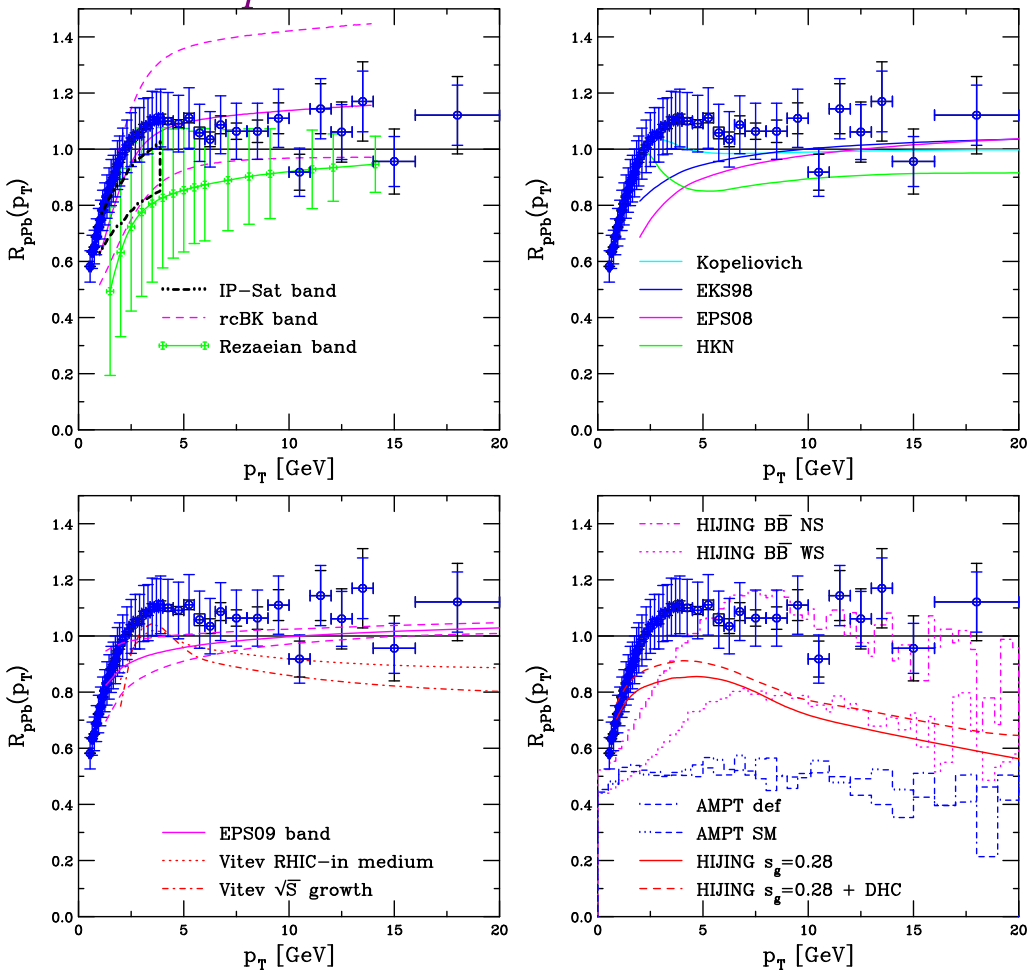

Figure 4: **Charged particle $R_{p\mathrm{Pb}}(p_T)$ calculations at $\sqrt{s_{_{NN}}} = 5.02$ TeV at $\eta \sim 0$ are compared to the ALICE data (Phys. Rev. Lett. 110 (2013) 082302). (Upper left) The bands from saturation models by Albacete *et al.* and Rezaeian (rcBK) and Tribedy & Venugopalan (IP-Sat) are compared to the ALICE data (Phys. Rev. Lett. 110 (2013) 082302). (Upper right) Results with more 'standard' shadowing by Barnafoldi *et al.* and Kopeliovich *et al.* are shown. (Lower left) The cold matter calculations by Vitev and collaborators include energy loss while those by Eskola and collaborators does not. (Lower right) HIJINGBB̄ (Topor Pop *et al.*) with and without shadowing compared to AMPT (Z. Lin) default and with string melting. The difference in the HIJING curves depends on whether the hard scatterings are coherent or not.**

Updates on $R_{p\mathrm{Pb}}$ at Midrapidity

The rcBK, b-CGC (Rezeian) calculation is adjusted by factor N multiplying $Q^2_{0,p}$ for midrapidity, behavior at other rapidities is now better predicted

EPS09 NLO (Eskola *et al*) agrees with ALICE and CMS data for $p_T < 20$ GeV but initial-state shadowing at such high scales cannot produce CMS rise at high p_T

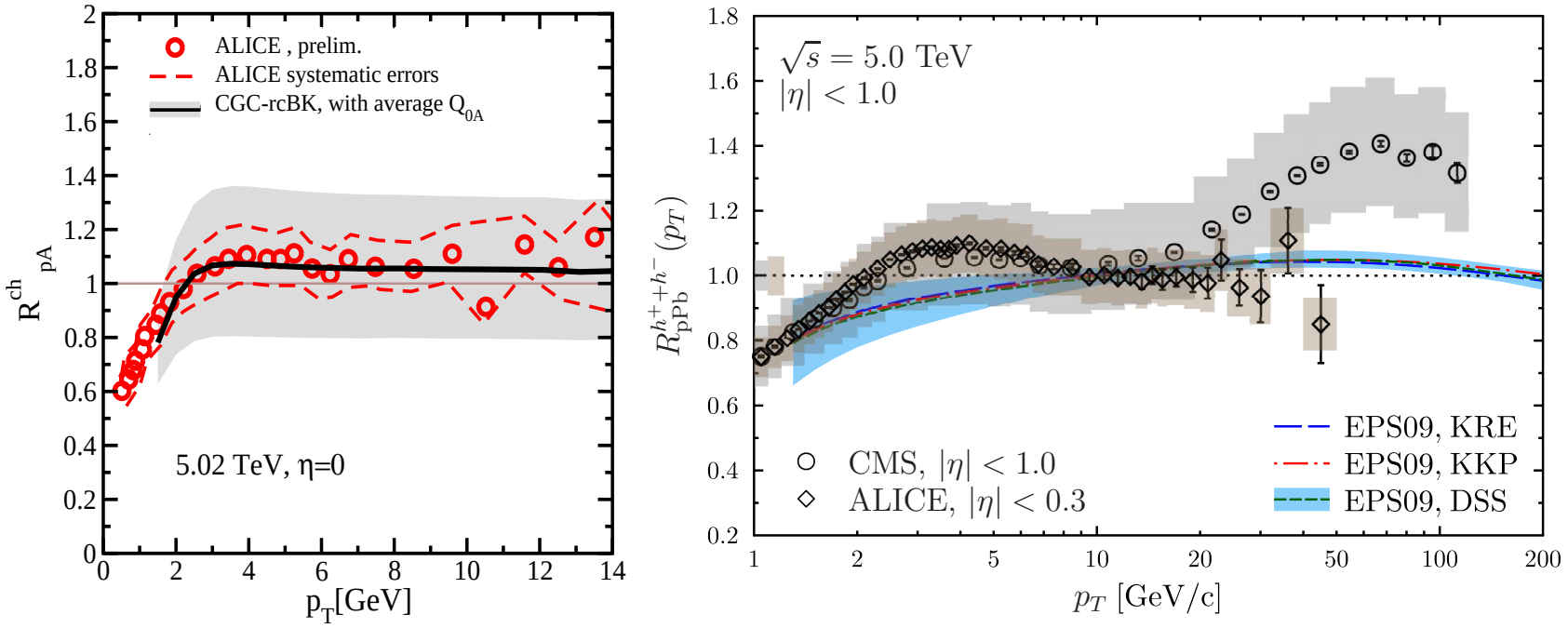

Figure 5: **Charged particle $R_{p\mathrm{Pb}}(p_T)$ calculations at $\sqrt{s_{NN}} = 5.02$ TeV at $\eta \sim 0$ are compared to the ALICE data (Phys. Rev. Lett. 110 (2013) 082302). (Left) The updated Rezaeian (rcBK) band, green curves on upper left of previous slide, adjusting range of N based on data – $R_{p\mathrm{Pb}}$ at other rapidities would be predictions. (Right) Results with EPS09 NLO modifications. The CMS data (Eur. Phys. J. C 75 (2015) 237) are shown to higher p_T.**

ALICE Charged Particle p_T Distributions

Results similar at low p_T but deviate significantly at higher p_T

AMPT agrees well with $p_T > 5$ GeV data, rcBK is better at low p_T, HIJINGB$\overline{\text{B}}$ is higher than data for $p_T > 3$ GeV

HIJING2.0 without shadowing better at low p_T, with better at high p_T

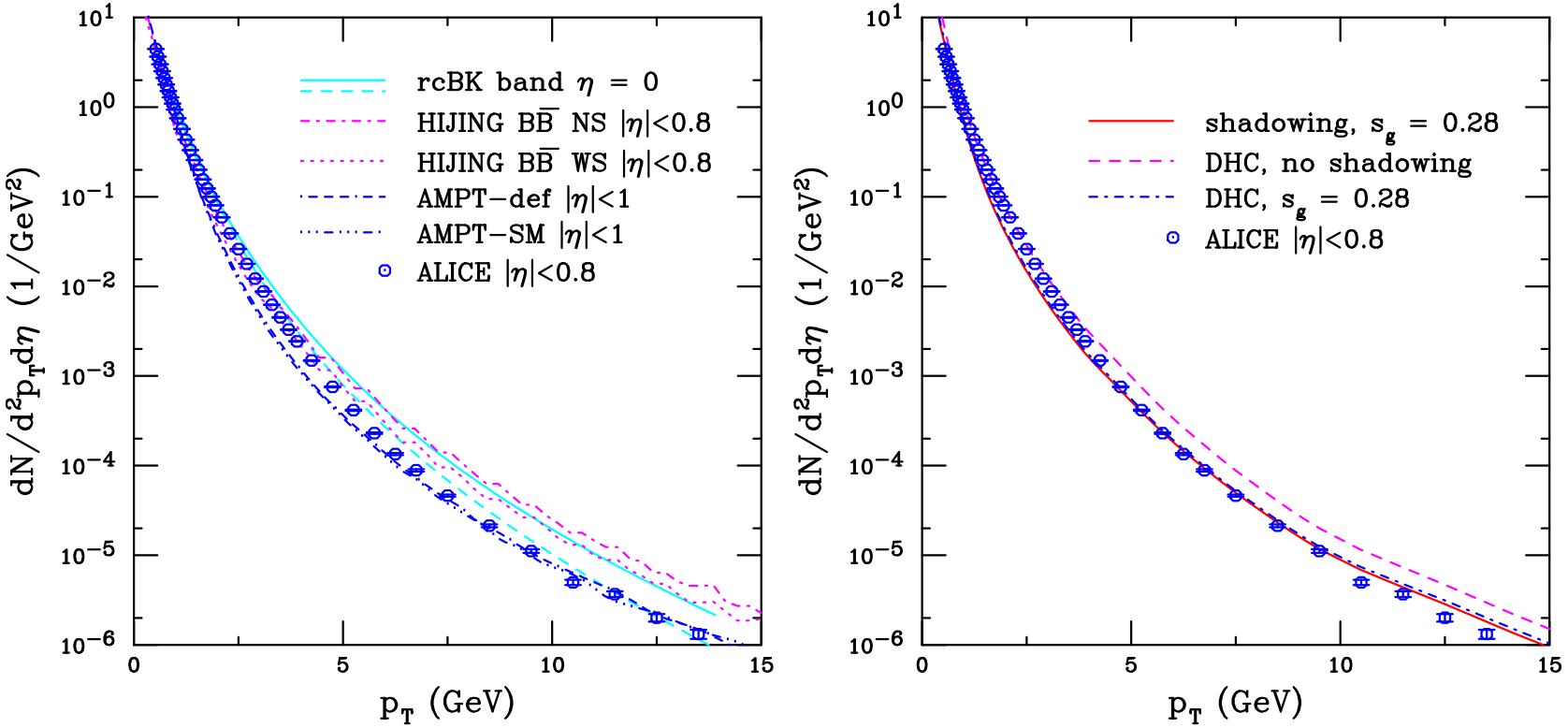

Figure 6: **(Left) Charged particle p_T distributions at $\sqrt{s_{NN}} = 5.02$ TeV. The solid and dashed cyan curves outline the rcBK band calculated by Albacete *et al.*. The magenta curves, calculated with HIJINGB$\overline{\text{B}}$2.0 are presented without (dot-dashed) and with (dotted) shadowing. The AMPT results are given by the dot-dash-dash-dashed (default) and dot-dot-dot-dashed (SM) blue curves. The data are from the ALICE Collaboration, Phys. Rev. Lett. 110 082302 (2013). (Right) The charged hadron p_T distribution in p+Pb collisions with different HIJING2.1 options is also compared to the ALICE data.**

CMS Charged Particle p_T Distributions

Agreement of calculations with CMS data similar as for ALICE data

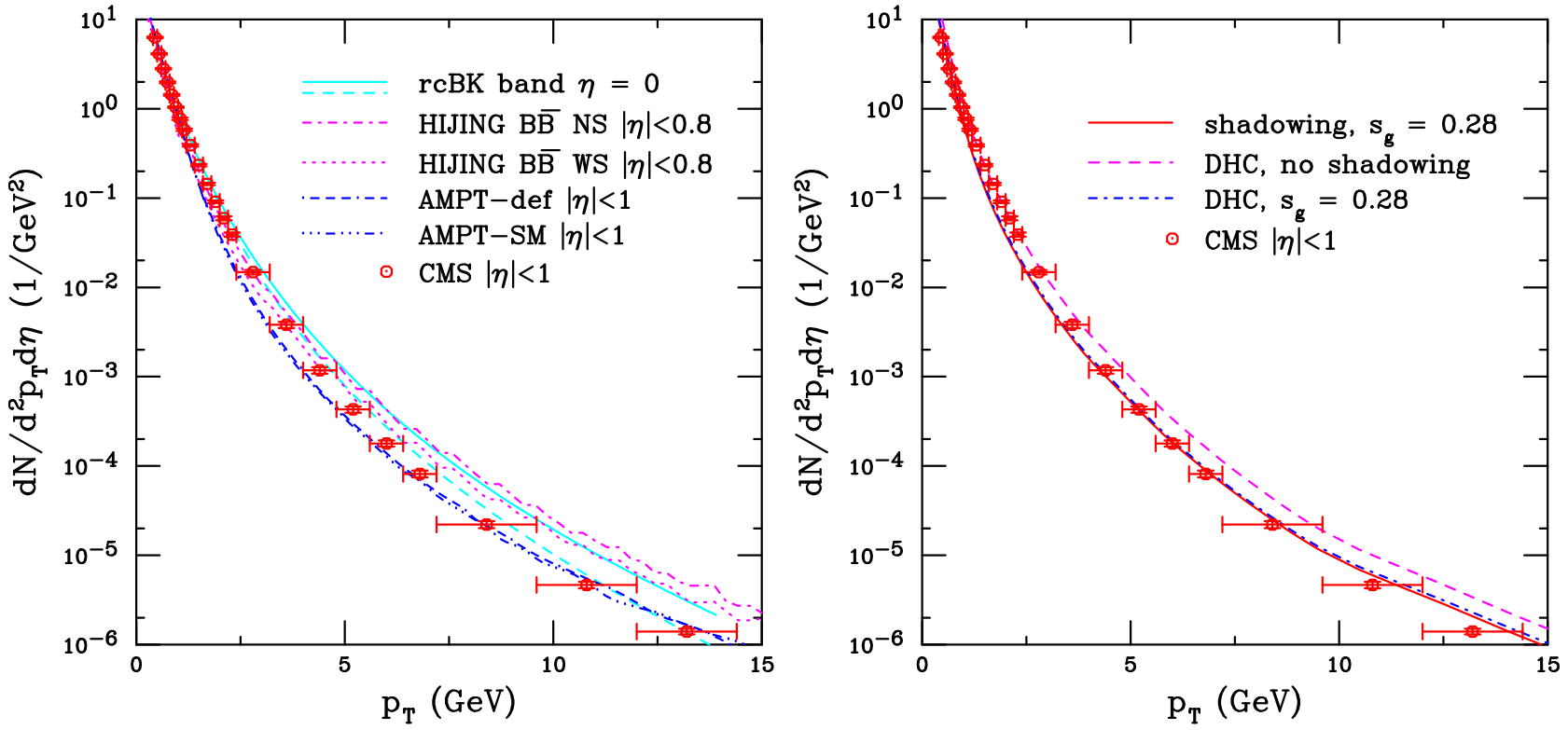

Figure 7: **(Left) Charged particle p_T distributions at $\sqrt{s_{NN}} = 5.02$ TeV. The solid and dashed cyan curves outline the rcBK band calculated by Albacete *et al.*. The magenta curves, calculated with HIJINGBB̄2.0 are presented without (dot-dashed) and with (dotted) shadowing. The AMPT results are given by the dot-dash-dash-dashed (default) and dot-dot-dot-dashed (SM) blue curves. The data are from the CMS Collaboration (Eur. Phys. J. C 75 (2015) 237). (Right) The charged hadron p_T distribution in p+Pb collisions with different HIJING2.1 options is also compared to the CMS data.**

Forward-Backward Asymmetry

$$Y^h_{\rm asym}(p_T) = \frac{E_h d^3\sigma^h_{p\rm Pb}/d^2p_T d\eta|_{\eta>0}}{E_h d^3\sigma^h_{p\rm Pb}/d^2p_T d\eta|_{\eta<0}} = \frac{R^h_{p\rm Pb}(p_T,\eta>0)}{R^h_{p\rm Pb}(p_T,\eta<0)}$$

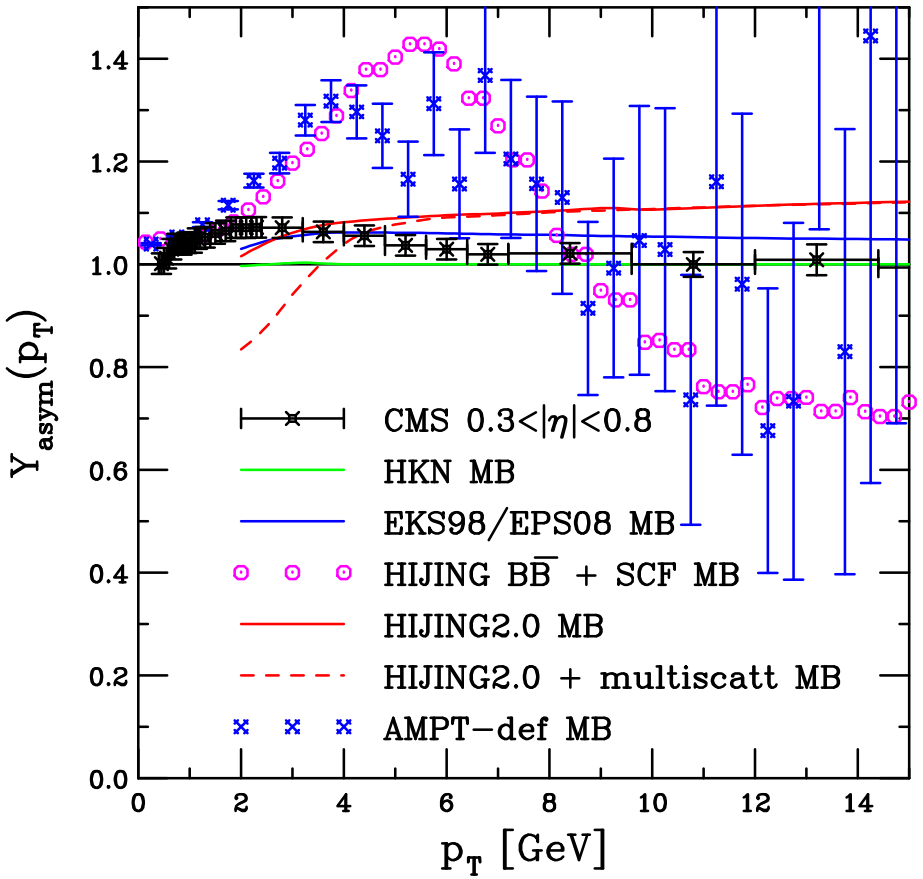

Figure 8: Predictions for the forward-backward asymmetry, $Y^h_{\rm asym}(p_T)$. Centrality independent results are shown for the HKN, EKS98 and EPS08 parameterizations (labeled MB). Minimum bias results are also shown for `HIJINGBB̄2.0` and `HIJING2.0` with multiple scattering. In addition, `HIJING2.0` results in MB collisions and for the 20% most central collisions are also shown. All these calculations were provided by Barnafoldi *et al.* The blue points are the `AMPT − def` results by Lin. The results are compared to the CMS data (Eur. Phys. J. C **75** (2015) 237) in the rapidity range $0.3 < y < 0.8$.

Flow

AMPT flow in good agreement with CMS data, note that the centrality criteria are not quite identical – the CMS data are in the range 0.5-2.5% centrality

Statistical uncertainties in calculations grows with p_T

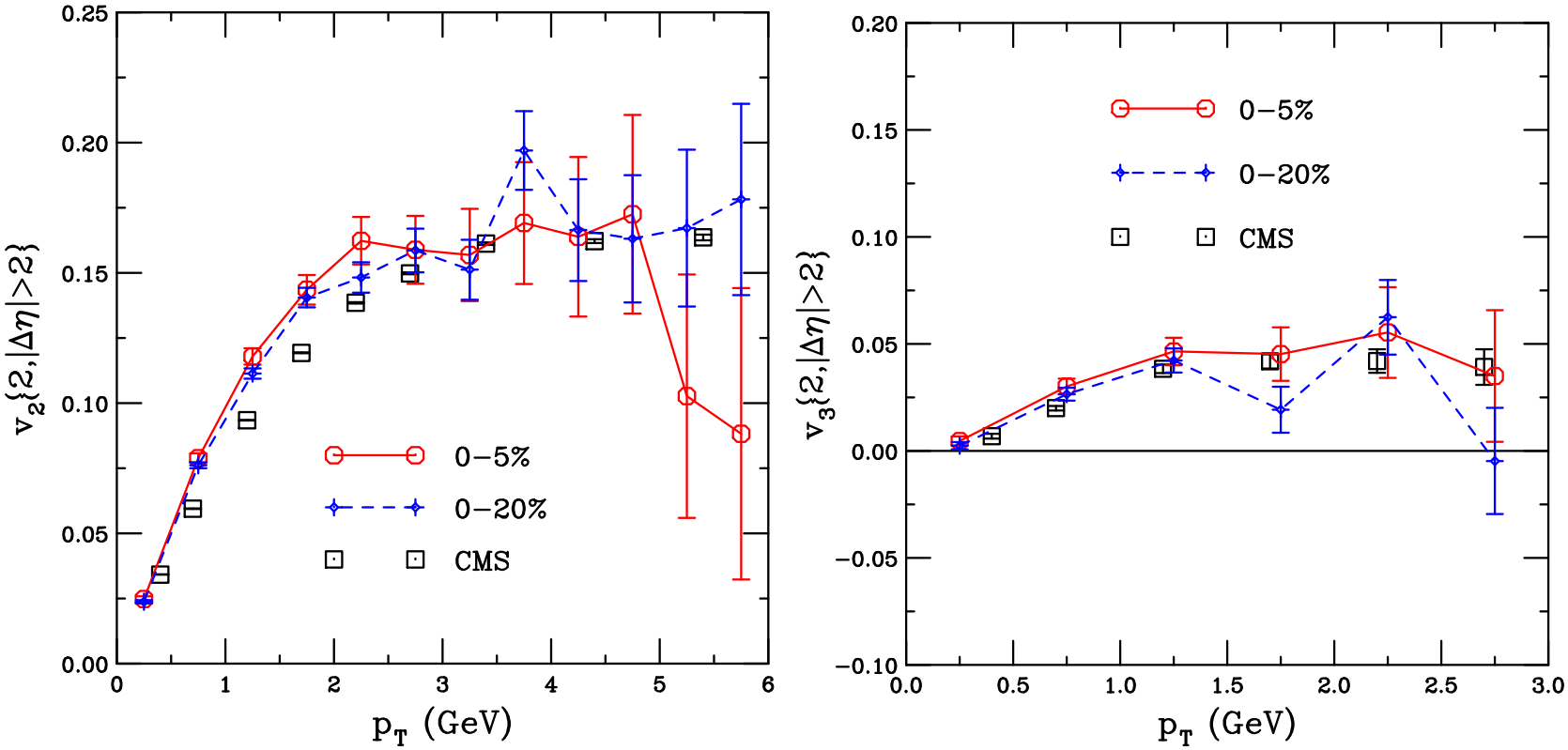

Figure 9: AMPT (Lin) predictions for flow are compared to the CMS data (Phys. Lett. B **724** (2013) 213).

Jets

Dijets with EPS09 NLO

Rapidity distribution (Eskola *et al*) shows clear shift

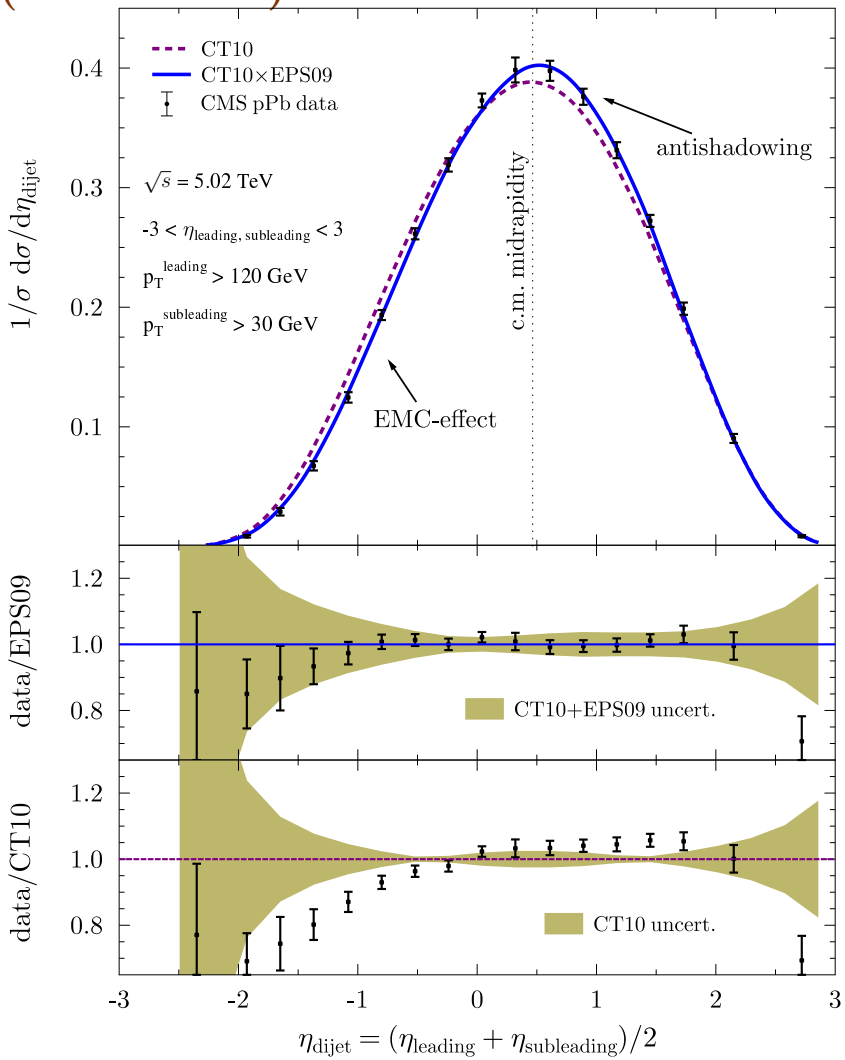

Figure 10: **The CMS dijet measurements (Eur. Phys. J. C 74 (2014) 2951) are compared to EPS09 NLO. The upper panel shows the normalized cross section as a function of η_{dijet}. The lower two panels display the ratio of the data to the CT10+EPS09 and CT10 calculations respectively, including the PDF and nPDF uncertainty bands.**

Single Inclusive Jet Production: Scaling With $p_T \cosh y$

The ATLAS data scale with $p_T \cosh y$ at forward rapidity, scaling becomes weaker at midrapidity and is broken at backward rapidity

Calculations by Kang, Vitev and Xing including cold matter energy loss exhibit the same scaling ($x_1 \propto p_T \cosh y$) but not the same curvature

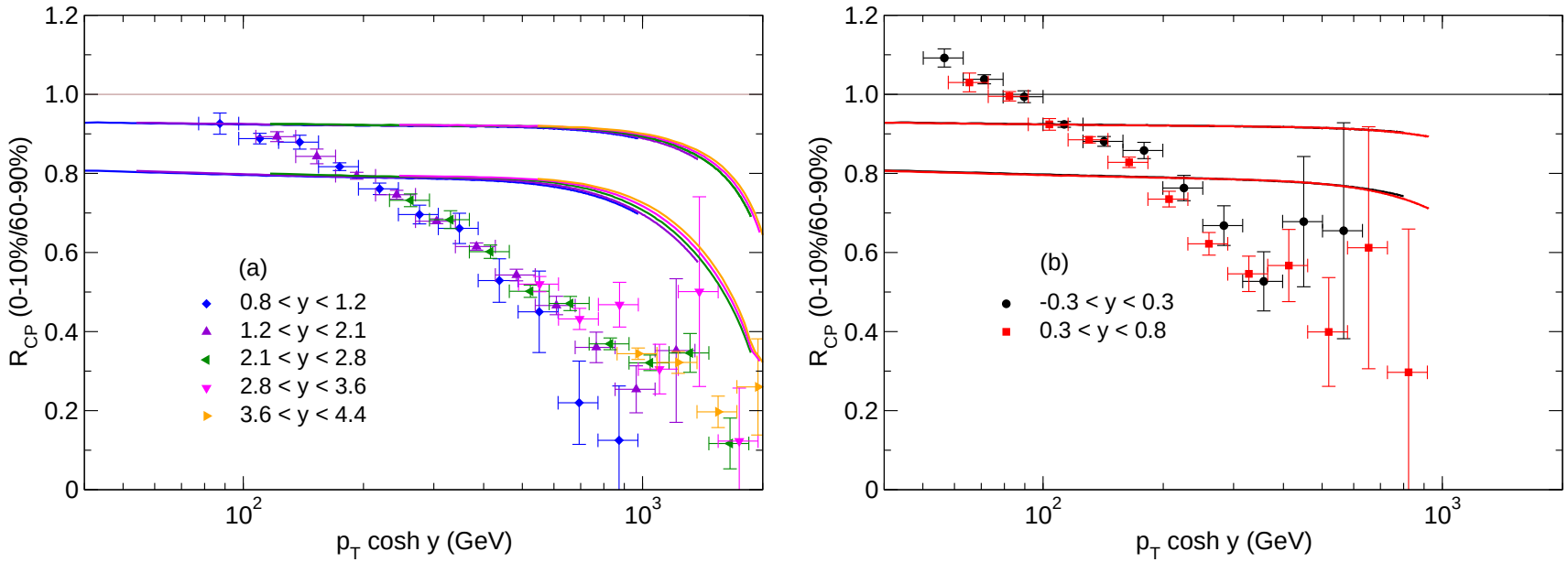

Figure 11: **Comparison of the calculated R_{CP} with the ATLAS data (Phys. Lett. B 748 (2015) 392) as a function of $p_T \cosh y$ by Kang *et al.*. In (a), the results at forward rapidities ($0.8 < y < 1.2$ (blue diamonds), $1.2 < y < 2.1$ (maroon upward-pointing triangles), $2.1 < y < 2.8$ (green left-pointing triangles), $2.8 < y < 3.6$ (magenta downward-pointing triangles), and $3.6 < y < 4.4$ (orange right-pointing triangles) are shown. In (b), results near midrapidity are shown ($-0.3 < y < 0.3$ (black circles) and $0.3 < y < 0.8$ (red squares)). The upper and lower limits of the calculation for each rapidity region overlap each other.**

J/ψ and Υ

Pinning Down Open Charm Uncertainties by Fitting $\sigma_{c\bar{c}}$

Caveat: full NNLO cross section unknown, could still be large corrections

Employ $m = 1.27$ GeV, lattice value at $m(3\,\mathrm{GeV})$ and use subset of $c\bar{c}$ total cross section data to fix best fit values of μ_F/m and μ_R/m

Result with $\Delta\chi^2 = 1$ gives uncertainty on scale parameters

LHC results from ALICE agrees well even though not included in the fits

Same mass and scale parameters used to calculate J/ψ

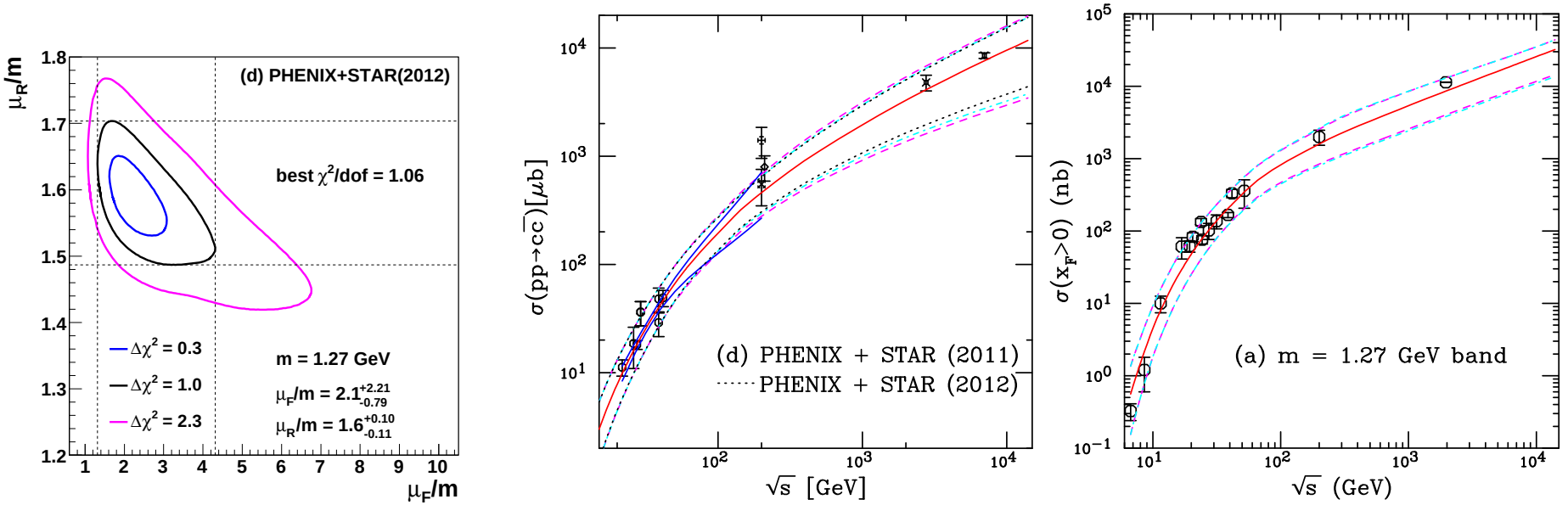

Figure 12: (Left) The χ^2/dof contours for fits employing the STAR 2011 cross section. The best fit values are given for the $\Delta\chi^2 = 1$ contours. (Center) The energy dependence of the charm total cross section compared to data. The best fit values are given for the furthest extent of the $\Delta\chi^2 = 1$ contours. The central value of the fit is given by the solid red curve while the dashed magenta curves and dot-dashed cyan curves show the extent of the corresponding uncertainty bands. The dashed curves outline the most extreme limits of the band. The dotted black curves show the uncertainty bands obtained with the 2012 STAR results while the solid blue curves in the range $19.4 \leq \sqrt{s} \leq 200$ GeV represent the uncertainty obtained from the extent of the $\Delta\chi^2 = 2.3$ contour. (Right) The uncertainty band on the forward J/ψ cross section. The dashed magenta curves and dot-dashed cyan curves show the extent of the corresponding uncertainty bands. The dashed curves outline the most extreme limits of the band. (Nelson, RV, Frawley, Phys. Rev. C **87** (2013) 014908)

Calculating Uncertainties in pA

The one standard deviation uncertainties on the quark mass and scale parameters calculated using EPS09 central set

If the central, upper and lower limits of $\mu_{R,F}/m$ are denoted as C, H, and L respectively, then the seven sets corresponding to the scale uncertainty are

$$(\mu_F/m, \mu_F/m) = (C,C), (H,H), (L,L), (C,L), (L,C), (C,H), (H,C)$$

The extremes of the cross sections with mass and scale are used to calculate the uncertainty

$$\sigma_{\rm max} = \sigma_{\rm cent} + \sqrt{(\sigma_{\mu,\rm max} - \sigma_{\rm cent})^2 + (\sigma_{m,\rm max} - \sigma_{\rm cent})^2}\ ,$$
$$\sigma_{\rm min} = \sigma_{\rm cent} - \sqrt{(\sigma_{\mu,\rm min} - \sigma_{\rm cent})^2 + (\sigma_{m,\rm min} - \sigma_{\rm cent})^2}\ ,$$

Uncertainties due to shadowing calculated using 30+1 error sets of EPS09 NLO added in quadrature, uncertainty is cumulative

Final-State Energy Loss (Arleo and Peigne)

Arleo and Peigne fit an energy loss parameter that also depends on L_A to E866 data and uses the same parameter for other energies

$$\frac{1}{A}\frac{d\sigma_{pA}(x_F)}{dx_F} = \int_0^{E_p-E} d\epsilon P(\epsilon)\frac{d\sigma_{pp}(x_F+\delta x_F(\epsilon))}{dx_F}$$

There is no production model, only a parameterization of the pp cross section

$$\frac{d\sigma_{pp}}{dp_T dx} = \frac{(1-x)^n}{x}\left(\frac{p_0^2}{(p_0^2+p_T^2)}\right)^m$$

Parameters n and m are fit to pp data, $n \sim 5$ at $\sqrt{s} = 38.8$ GeV, 34 at 2.76 TeV

Including shadowing as well as energy loss modifies the energy loss parameter, no significant difference in shape of fit at fixed-target energy but significant difference at higher $\sqrt{s}$

Backward x_F/y effect is large for this scenario

Other Calculations (Lansberg, Ferreiro and Fujii)

Lansberg and collaborators use LO color singlet model (CSM) to calculate production

Using LO CSM modifies R_{pA} relative to LO CEM due to shadowing because LO CEM has $p_T = 0$ for the J/ψ (y dependence only), other differences include mass and scale values used

Uncertainites in the shadowing result shown are from two particular EPS09 sets that give the minimum and maximum magnitudes of gluon shadowing, not from taking all sets in quadrature

Ferreiro calculates the difference between J/ψ and ψ' production in the comover interaction model

No absorption by nucleons is included but EPS09 LO shadowing is employed

The comover interaction cross section is larger for ψ', leading to the differences observed

CGC calculations by Fujii *et al.* are made only in the forward direction where x_2 (in Pb nucleus) is small

Uncertainty comes from varying the saturation scale, $Q^2_{0\mathrm{sat},A} \sim (4-6)Q^2_{0\mathrm{sat},p}$ and the quark masses, $1.2 < m_c < 1.5$ GeV and $4.5 < m_b < 4.8$ GeV

$R_{p\mathrm{Pb}}(y)$ for J/ψ

NLO shadowing does not describe curvature of data, LO band is larger due to greater uncertainty of EPS09 LO (only min/max used in Lansberg calculation)

Energy loss with shadowing (not shown) overestimates effect at forward rapidity

CGC + CEM (Fujii) below data, CGC + NRQCD (not shown) may agree better

EPS09 NLO and LO differ due to low x behavior of CTEQ6M and CTEQ61L

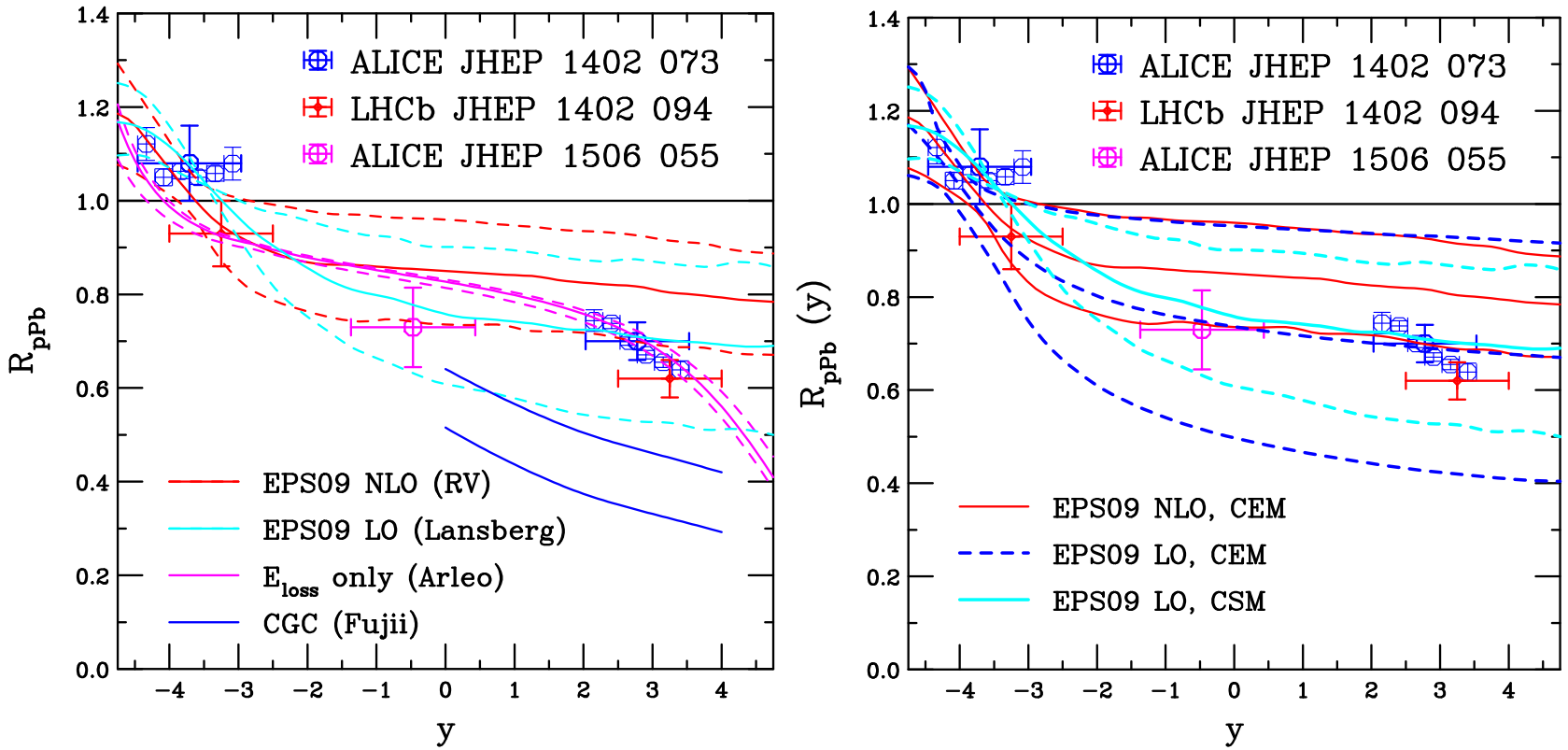

Figure 13: **(Left) The $R_{p\mathrm{Pb}}$ ratio for J/ψ as a function of y. The dashed red histogram shows the EPS09 NLO CEM uncertainties. The EPS09 LO CSM calculation by Lansberg *et al.* is shown in cyan. The energy loss calculation of Arleo and Peigne is shown in magenta. The upper and lower limits of the CGC calculation by Fujii *et al* are in blue at forward rapidity. (Right) The EPS09 LO calculations in the CEM (blue) and CSM (cyan) are compared. The CEM calculation includes the full EPS09 uncertainty added in quadrature while the CSM calculation includes only the minimum and maximum uncertainty sets. The EPS09 NLO CEM result is in red. The ALICE and LHCb data are also shown.**

$R_{FB}(y)$ and $R_{FB}(p_T)$ for J/ψ

Forward $(+y)$ to backward $(-y)$ ratio preferable because no pp normalization required for data

Data are flatter in y than the calculations

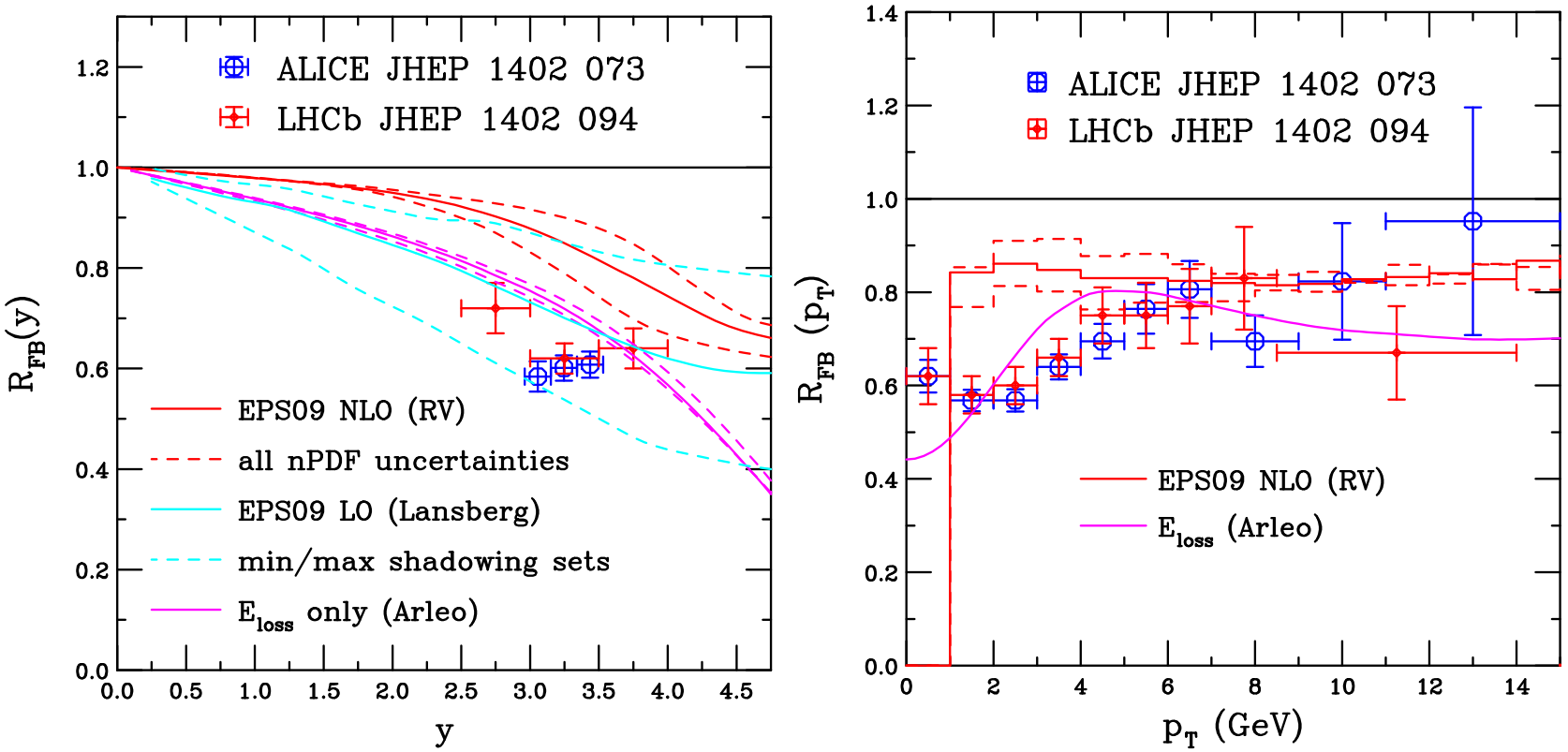

Figure 14: **The forward-backward ratio $R_{F/B}$ is shown for J/ψ as a function of y (left) and p_T (right). The dashed red histogram shows the EPS09 NLO CEM uncertainties. The energy loss only calculations of Arleo and Peigne is shown in magenta. The ALICE and LHCb data are also shown.**

$R_{p\mathrm{Pb}}(y)$ for J/ψ and ψ' in Comover Approach

$$R^{\psi}_{pA}(b) = \frac{\int \mathrm{d}^2 s\, \sigma_{pA}(b)\, n(b,s)\, S^{sh}_{\psi}(b,s)\, S^{co}_{\psi}(b,s)}{\int \mathrm{d}^2 s\, \sigma_{pA}(b)\, n(b,s)}$$

Comover interaction cross sections taken from earlier results

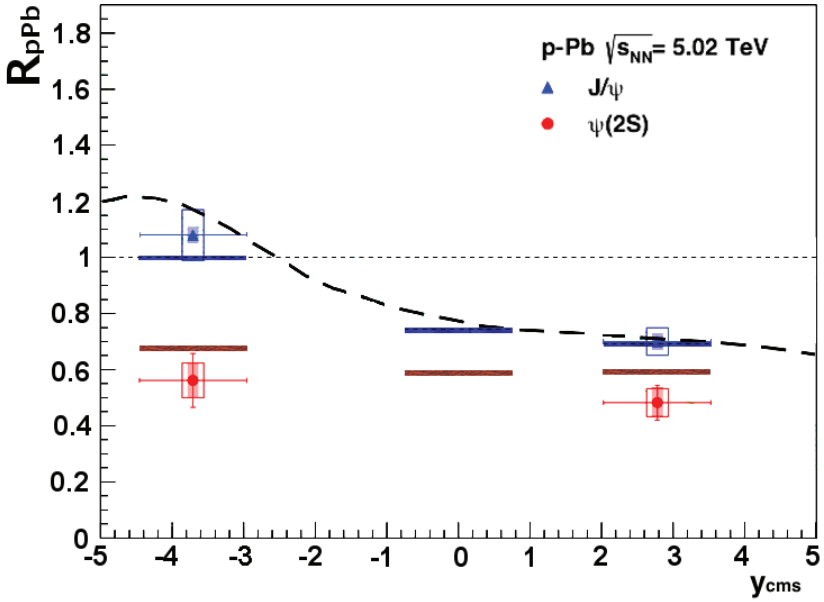

Figure 15: **The J/ψ (blue lines) and $\psi(2S)$ (red lines) nuclear modification factor R_{pPb} as a function of rapidity compared to the ALICE data (JHEP 1412 (2014) 073). The suppression due to shadowing alone (dashed line) is also shown. The ALICE results are given by the points.**

$R_{p\mathrm{Pb}}(y)$ and $R_{F/B}(y)$ for Υ

Shadowing reduced in all cases for the Υ due to the larger mass scale

Interestingly, the CGC result still gives relatively large suppresssion at this high scale, presumably $m_b > Q_{0\mathrm{sat},A}$?

Significant difference between ALICE and LHCb data

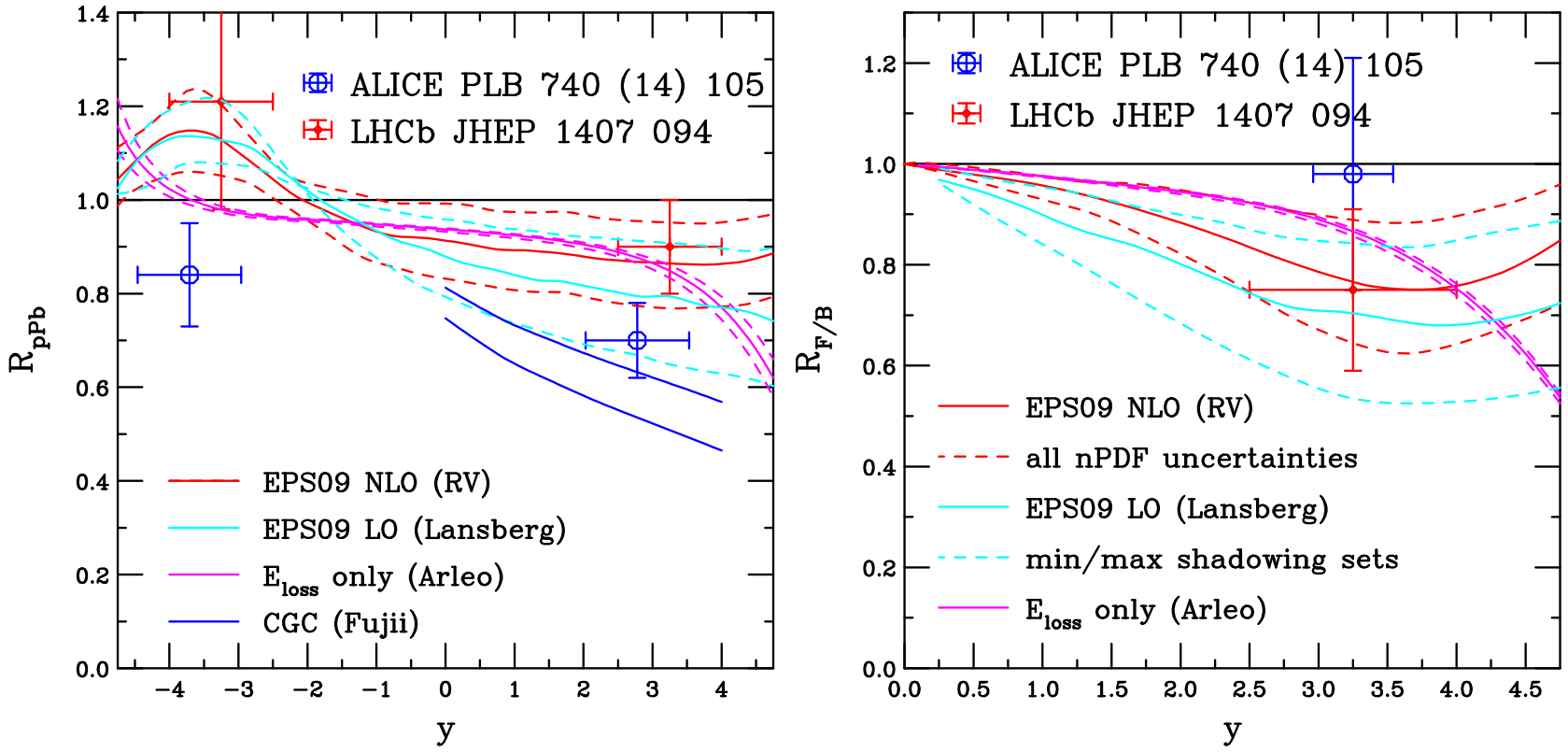

Figure 16: **(Left) The $R_{p\mathrm{Pb}}$ ratio for Υ as a function of y. The dashed red histogram shows the EPS09 NLO CEM uncertainties. The EPS09 LO CSM calculation by Lansberg *et al.* is shown in cyan. The energy loss calculation of Arleo and Peigne is shown in magenta. The upper and lower limits of the CGC calculation by Fujii *et al* are in blue at forward rapidity. (Right) The forward-backward ratio for Υ production as a function of rapidity. The same calculations are shown here except that there is no CGC result in the backward region. The ALICE and LHCb data are also shown.**

Z^0 bosons

Dependence on p_T and y

NLO pQCD calculations (BW Zhang *et al.*) reproduces the p_T and y dependence of the ATLAS and CMS data although rapidity distribution of CMS is somewhat better described

Calculation is done assuming that the proton beam moves to postive rapidity

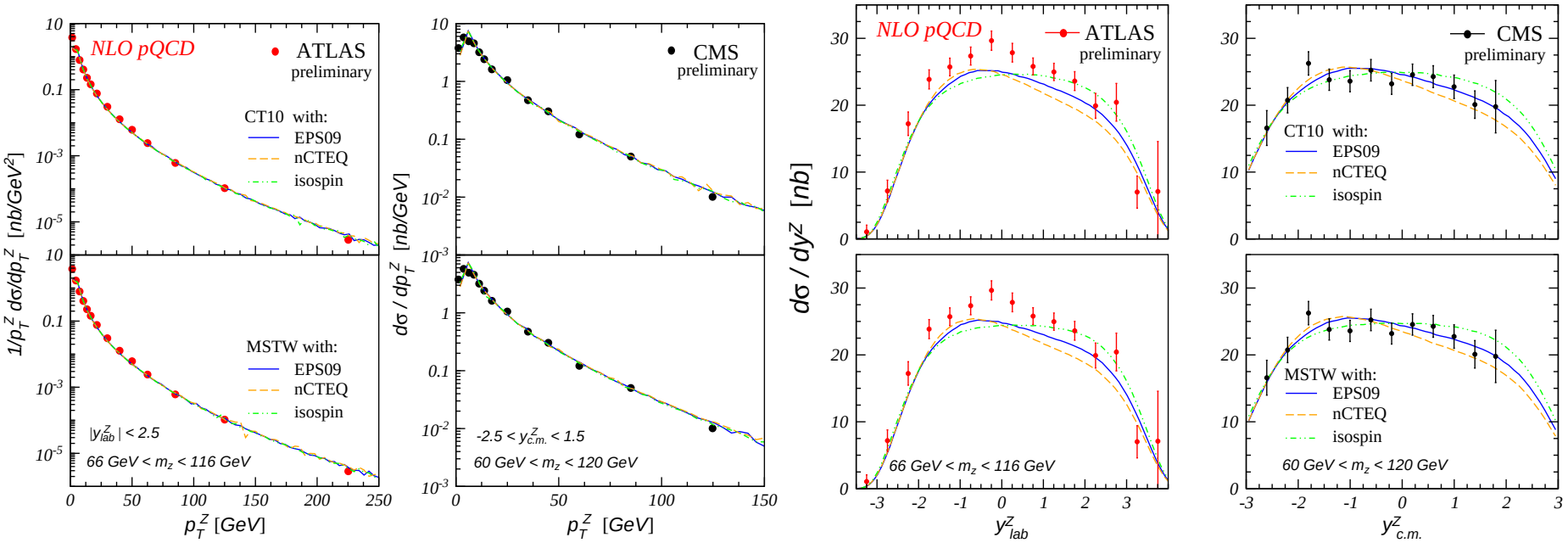

Figure 17: The differential cross section of the Z^0 rapidity in p+Pb collisions at $\sqrt{s_{NN}} = 5.02$ TeV. The left panels show the results for ATLAS (Nucl. Phys. A **931** (2014) 617) while the right show those for CMS (Nucl. Phys. A **931** (2014) 718). The top panel results are calculated with CT10 PDFs, while the bottom are calculated with MSTW2008. The left-hand side shows the p_T distributions while the rapidity distributions are on the right-hand side.

Forward-Backward Asymmetry

The forward-backward asymmetry for CMS, near midrapidity, is well reproduced

The LHCb data, at higher rapidity, are not well reproduced at backward rapidity so that the calculations give a larger asymmetry than the data

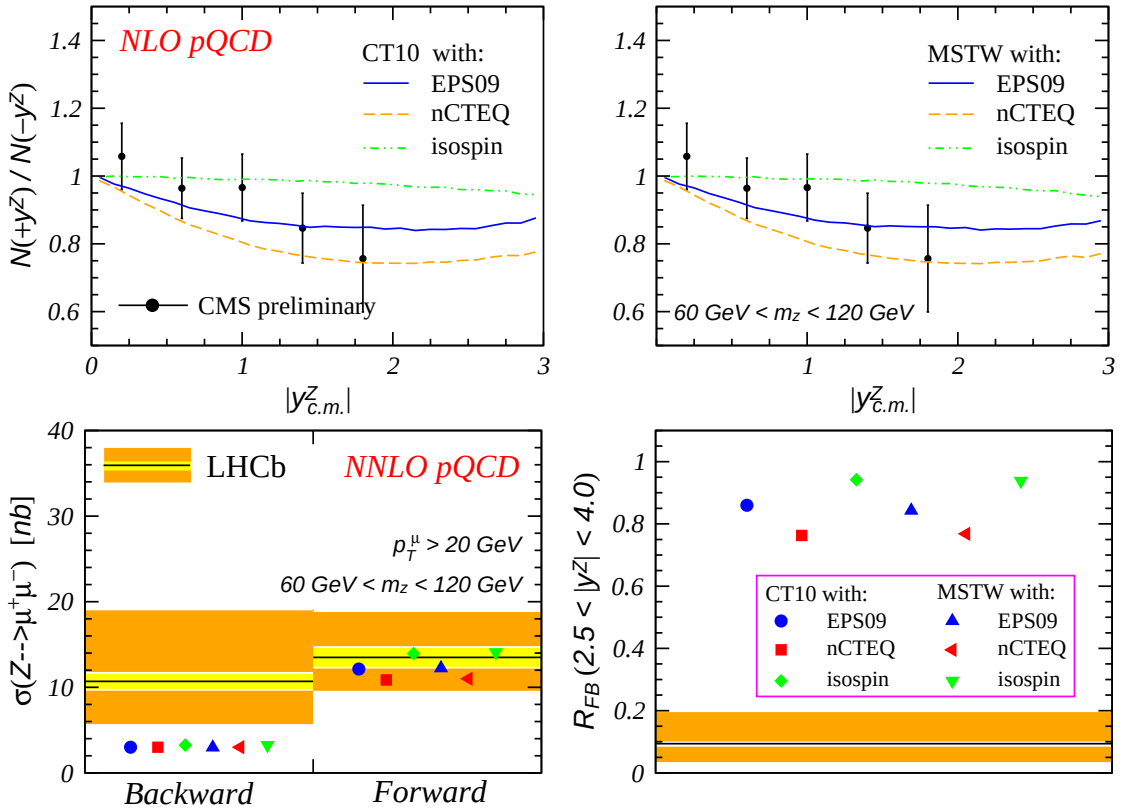

Figure 18: The forward-backward asymmetry, as a function of the absolute value of Z^0 rapidity in the center of mass frame in p+Pb collisions at $\sqrt{s_{NN}} = 5.02$ TeV. (Top) The results with the CT10 (left) and MSTW2008 PDFs (right) are shown with the CMS data (Nucl. Phys. A **931** (2014) 718). (Bottom) The forward and backward cross sections (left) and forward-backward asymmetry (right) for Z^0 production in LHCb (JHEP **1409** (2014) 030).

Summary

- p+Pb run at LHC provides critical studies of cold matter effects in a new energy regime
- The charged particle results for $R_{p\mathrm{Pb}}$ are mostly compatible with pQCD and CGC results, $dN_{\mathrm{ch}}/d\eta$ more difficult to reproduce
- The J/ψ and Υ results are compatible with both shadowing only and energy loss only but not really with CGC+CEM
- Dijet and gauge boson results under good control although LHCb forward-backward Z^0 ratio at higher rapidity more difficult to explain with calculations
- Thanks again to everyone who provided predictions and data!